PHYSICAL REVIEW E, VOLUME 65, 016408

Local and fast relaxation phenomena after laser-induced photodetachment in a strongly electronegative rf discharge

M. Yan,* A. Bogaerts, and R. Gijbels
Department of Chemistry, University of Antwerp (UIA), Universiteitsplein 1, B-2610 Wilrijk-Antwerp, Belgium

W. J. Goedheer
FOM-Institute for Plasma Physics "Rijnhuizen," P.O. Box 1207, 3430 BE Nieuwegein, The Netherlands
(Received 12 April 2001; revised manuscript received 2 August 2001; published 17 December 2001)

A one-dimensional self-consistent particle in cell/Monte Carlo method is used to study the local (at the laser impact region) and fast relaxation phenomena after laser-induced photodetachment in a strongly electronegative SiH_4/H_2 rf discharge. The relaxation process of the local densities of the charged plasma species has been studied in association with the time evolution of the local electric field. The phenomena predicted theoretically about the relaxation processes, such as the potential well, the electrostatic oscillation, the long lasting potential structure, the distortion of the early potential perturbation on the measurement of negative ion temperature, and the depression in the positive ion density profile at the edges of the laser impact region, have been confirmed by our simulation results. Compared to the relaxation in weakly electronegative discharges, the local and even the global electric field in strongly electronegative discharges, has been weakened strongly after photodetachment. The relaxation of the local electric field lasts 100 rf cycles with the recovery of the local electron density and the local electron energy. The electrostatic oscillation exhibited as the deviation in quasineutrality, is very strong and continues over several rf cycles in our case. The large dip in the center of the positive ion density profile, observed in the experiment, is also reproduced by our model.

DOI: 10.1103/PhysRevE.65.016408 PACS number(s): 52.25.Dg, 52.80.−s

I. INTRODUCTION

Laser-induced photodetachment is a widely used technique to measure the density, thermal energy, and velocity of negative ions in electronegative rf discharges (e.g., [1,2] and references therein). Since the negative ion density is obtained from the measured density of the detached electrons, and since the thermal energy of the negative ions can be deduced from the relaxation of the negative ion density at the laser impact region, it is essential to understand the relaxation mechanisms of the electrons and negative ions.

The relaxation process after photodetachment has the following characteristics [3].

(1) The laser pulse only changes the relative ratio between electron and negative ion density but does not produce any net charge.

(2) The start mechanism of relaxation is driven by the fluxes resulting from the density gradients of electrons and negative ions.

(3) The basic transport process, dominating the relaxation is ''monopolar'' drift. The charged particles with the same sign preserve local neutrality by counterflowing. This is the opposite process from the well-known ambipolar drift, which involves species with opposite charges flowing in the same direction.

Theoretical studies in the past [3–7] have been performed under the following conditions.

(1) The plasma contains a low fraction of negative ions, such as in H_2 discharges (weakly electronegative discharges). The influence of the extra electrons after photodetachment on the original electron density can, hence, be regarded as only a small perturbation.

(2) The plasma is collisionless.

(3) The extra electrons have more or less the same energy as the background electrons.

(4) Charge neutrality is assumed.

(5) Only dc discharges have been considered.

In contrast to the above studies, we investigate the relaxation phenomena after photodetachment in a strongly electronegative discharge, which is widely used in deposition or etching. The conditions after photodetachment in such a discharge are different from the ones mentioned above.

(1) The ratio between electron and negative ion densities is lower than $\frac{1}{10}$. After photodetachment, the extra electron density could be more than ten times higher than the original electron density. Hence, it cannot be considered as a small perturbation.

(2) The detached electrons cannot be heated up quickly because the bulk electric field is dramatically weakened compared to the original strong field in such kind of discharges.

(3) The mean free path λ is less than 1 mm, whereas the discharge dimension is about several centimeters, consequently collision effect should be considered.

(4) Since the Debye length is about 1 mm, which is comparable with the characteristic scale of the laser-induced perturbation (several millimeters), the local quasineutrality can be broken.

(5) The radio frequency (rf) discharges operate at 13.56 MHz, and the temporal dynamics of the plasma potential and photodetachment signals have the same time scale.

In this paper, we study the local relaxation phenomena after photodetachment in strongly electronegative SiH_4/H_2 rf

*Email address: yan@uia.ua.ac.be

discharges by a one-dimensional (1-D) particle in cell/Monte Carlo (PIC/MC) model. The current work is an extension of our previous work [8], which mainly concerned the global relaxation mechanism (i.e., interpreted over the whole plasma region) and at a rather large time scale (about ten rf cycles). The relaxation is a global effect as shown in [8]. However, in order to interpret the experimental results, especially in case of probe measurements [9–13], the local effects are important to be understood. Moreover, to have correct assumptions for theoretical models such as for the determination of the temperature of negative ions from the measured data [3,7,9], it is necessary to have a good understanding of the local and fast relaxation phenomena. We refer to the relaxation at the laser impact region as local relaxation in this paper.

We use a self-consistent kinetic 1D PIC/MC model developed specifically for discharges in SiH_4/H_2 [14] to simulate and focus on the local relaxation after photodetachment. The SiH_4/H_2 rf discharge serves as an example to qualitatively demonstrate the characteristics of the local relaxation process after photodetachment in strongly electronegative discharges. The results obtained in this paper can be generalized to other strongly electronegative discharges. We focus on the understanding of the local fast relaxation of the densities, the average energy, the energy distribution function (EDF) of the charged particles, the charge quasineutrality, and the electric field. From the results, we can confirm some theoretical predictions in the relaxation process, such as the potential well [2,7,15] and its sign reversal [7], the electrostatic oscillation [2,7], the long lasting potential structure associated with the perturbation in the electron density [7], and the distortion of the early potential on the measurement of negative ion temperature [7]. We will also compare the difference in the local relaxation between weakly and strongly electronegative discharges, such as the long time recovery of the electron energy, the electron energy distribution function (EEDF), and the electric field in the latter kind of discharges.

II. MODEL DESCRIPTION

The PIC/MC method is based on a kinetic description of the particle motion in phase space. Charged ''superparticles'' move in the self-consistent electric field that they generate. A Monte Carlo formalism is used to describe the collisions. This method simulates the behavior of the particles on the lowest microscopic level, and it does not make use of many assumptions. Detailed descriptions of the PIC/MC method can be found, e.g., in Refs. [16,17].

We study the relaxation phenomena after photodetachment in SiH_4/H_2 discharges. Four types of charged species, [i.e., electrons (e^-), positive ions (SiH_3^+, H_2^+), and negative ions (SiH_3^-)], are taken into account. This is justified by measurements [18] and by results from fluid modeling where a large number of species was considered [19]. The electron impact collisions included in the model are elastic collisions, vibrational excitation, electron attachment, dissociation, and ionization [14]. The ion impact collisions are elastic collisions, charge transfer, and positive-negative ion recombination [14].

The initial conditions and assumptions for the simulations are the following.

(1) A laser pulse is fired at the beginning of an rf cycle after the discharge has reached periodic steady state, and the pulse duration is neglected. The process is considered to be one dimensional. The laser beam is assumed to be infinite in the directions parallel to the electrodes.

(2) The laser intensity profile is assumed to have a rectangular shape because in the experiments [3,7,9], the laser intensity is large enough to depopulate the local negative ions completely. Moreover, the radius of the laser beam is normally controlled by diaphragms [7,9], hence, the real Gaussian distribution of the laser intensity will be cutoff into a rectanglelike shape.

(3) The only laser-induced reaction considered is photodetachment, $SiH_3^- + h\nu \rightarrow SiH_3 + e^-$. The electron affinity of SiH_3 is 1.4 eV [20]. All the detached electrons have an energy of 0.2 eV, which is the difference between the assumed photon energy (1.6 eV) and the electron affinity.

(4) The negative ion density (SiH_3^-) in the laser impact region drops 100% due to the photodetachment, and the same amount of electrons is released at exactly the same position. The positive ion (SiH_3^+ and H_2^+) density does not change during the laser pulse.

The distance between the two electrodes is 3 cm. In order to have a clear view of the local relaxation phenomena, we chose the laser injection point at the discharge center that is characterized by a high plasma density. The laser beam width is 2 mm. The laser impact region is thus from 1.4 cm to 1.6 cm. 2 mm is typically what is used in experiments to obtain a reasonable spatial resolution. It should be noted that in this paper the term ''local'' refers to the variables at the laser impact position.

The typical relaxation phenomena are demonstrated for a discharge with an applied rf frequency of 13.56 MHz and an applied voltage of 200 V, at a gas pressure of 400 mTorr. The background gas density (feed gas) is regarded as uniform and the gas pressure is fixed during the simulation. The mean free path λ is about 0.1 mm, which is much smaller than the discharge scale of 3 cm. The averaged energy of the original electrons is about 3 eV, which is much higher than the ion energy, and the electron density is about $10^{15}\,m^{-3}$. These give rise to a Debye length λ_D of about 0.5 mm, which has the same order of magnitude as the laser beam width of 2 mm.

The ratio of SiH_4 and H_2 partial pressures is set to 1:9 in order to have a large amount of H_2^+ ions, as we want to see the influence of an extra type of positive ions on the relaxation. The secondary electron emission coefficient and the reflection coefficient from the electrodes are assumed to be zero. In the simulations we use 120 spatial grid points and 1000 time steps in one rf cycle. For each type of charged particle (i.e., e^-, SiH_3^+, H_2^+, and SiH_3^-) 3000–7000 ''superparticles'' are followed. In order to reduce the fluctuation in the simulation, the results are obtained by averaging over many simulations. A new simulation is generated by extending the unperturbed phase prior to the detachment event with

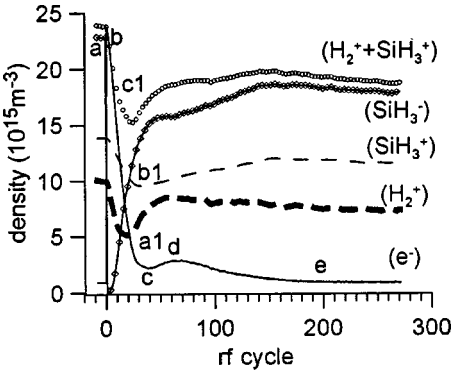

FIG. 1. Evolution of the species densities at the laser impact position as a function of number of rf cycles. The letters *a*, *b*, *c*, *d*, *e*, *a*1, *b*1, and *c*1 indicate different moments in the recovery of the electron density and the positive ion densities.

one rf cycle. The results with respect to the evolution of the calculated plasma quantities as a function of rf cycle (e.g., Fig. 1) are normally averaged over ten simulations and those about the spatial profiles of the quantities at different times [e.g., Fig. 2(b)] are averaged over 80 simulations.

In strongly electronegative discharges, the bulk field changes strongly as a function of time in the rf cycle [21,22], and the electrons have a light mass so that they can see this varying field. Therefore, in order to investigate the relaxation taking into account the effect of the bulk field (which is considerable at the beginning of the rf cycle), the results in this paper are taken at the beginning of each rf cycle, if not specified otherwise.

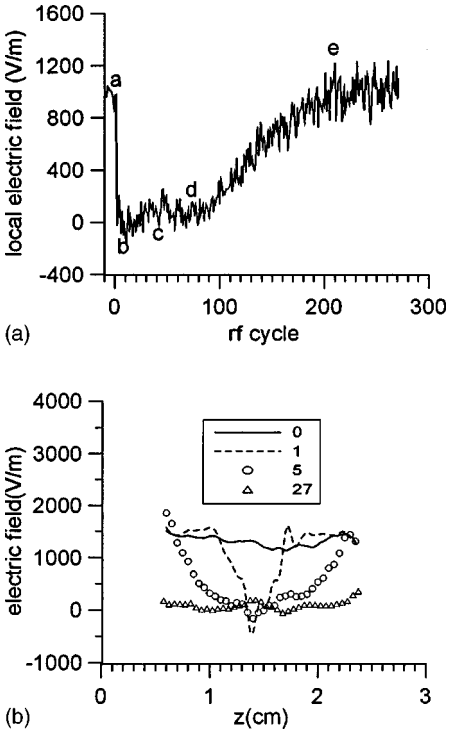

FIG. 2. (a) Evolution of the local electric field. The letters *a*, *b*, *c*, *d*, and *e* indicate different moments, at the same time as in the recovery of the electron density. (b) Spatial profile of the bulk electric field after 0, 1, 5, and 27 rf cycles.

III. RESULTS AND DISCUSSION

A. Relaxation of local charged particle densities and electric field after photodetachment

Figure 1 shows the evolution of the charged particle densities (e^-, SiH_3^+, H_2^+, SiH_3^-, and the sum of SiH_3^+ and H_2^+) averaged over the laser impact region (2 mm) after photodetachment. The key to explain this evolution is the relaxation of the local electric field and the electric field profile [Figs. 2(a) and 2(b)]. The letters $a-e$ and $a1-c1$ in the figures indicate the transition between several characteristic phases during the relaxation. Unless specified otherwise, the letters marked in one figure are independent on the letters in the other figures. The negative values at the *x* axis stand for rf cycles before the photodetachment takes place. ''0'' means that the results are sampled immediately after the photodetachment.

a. Initial situation. Point ''*a*'' at ''0'' rf cycle in Fig. 1 indicates the starting point just after photodetachment. There is a jump in the local e^- density and a dip in the local SiH_3^- density as stated in the assumptions above. The SiH_3^+, H_2^+ densities (in Fig. 1), and the electric field [in Fig. 2(a)] do not change instantaneously.

b. Period of fast changes. From ''*a*'' to ''*b*'' in Fig. 1 (several rf cycles), it can be seen that the electron and SiH_3^- densities start to recover but the recovery speed of the local electron density is larger than that of SiH_3^-. At the same time the local positive ion densities also change strongly. The initial driving mechanisms of the relaxation [3] are the smoothening of the density gradients across the edge of the laser impact region at the thermal velocities of the two negative species. However, since the electrons have a much higher mobility, the motion of electrons is faster than that of negative ions. This leads to a charge separation and hence an electric field [see the curve after one rf cycle in Fig. 2(b)]. This field lowers the electron flux and accelerates the smoothening of the negative ion density. This transport process occurs in a multispecies plasma and is the so-called ''monopolar'' drift, in which particles with the same charge sign preserve local neutrality by counterflowing. This is the opposite process of the well-known ambipolar drift that involves species with opposite charge, flowing in the same direction [3]. Simultaneously, however, this field also forces the positive ions to move in the same direction as the electrons, which is ''ambipolar'' drift. Since the density gradients of the electrons and negative ions at the edges of the laser impact region are initially extremely strong, a strong change of the electric field and hence a strong decrease of the positive ion density is expected at the edges. Indeed, Fig. 3 shows two sharp dips (points ''*a*'' and ''*b*'' at the two edges) in the H_2^+ density profile (dashed line) after one rf cycle. The ions that have been removed from the edges are pushed away and appear back as two peaks (points ''*c*'' and ''*d*'') a bit further away from the laser impact position. The dip of positive ion density at the edges in weakly electronegative discharges has been predicted analytically [5]. We have also found that the positive ions respond quickly to the strong electric field that is created at time ω_{pe}^{-1}. As a result, the local positive ion density already decreases after one rf cycle,

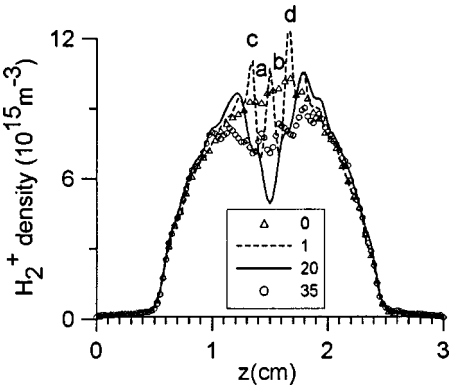

FIG. 3. H_2^+ density profile after 0, 1, 20, and 35 rf cycles.

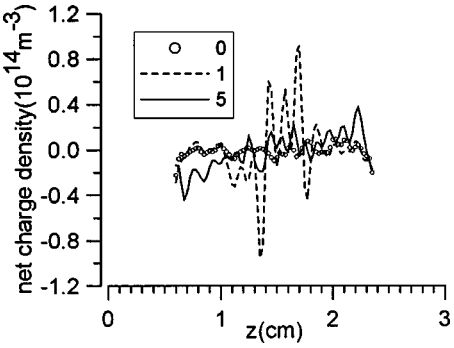

FIG. 4. Spatial profile of the net charge density in the plasma bulk after zero, one, and five rf cycles.

as shown in Fig. 1. Note that the time step in Fig. 1 is one rf cycle.

The electric field varies strongly during this period, as shown in Fig. 2(b). The change of the electric field in the laser impact region differs from the outside region. The different characteristics of the electric field along the discharge can be understood as follows. The motion of the charged particles is described by the macroscopic equation

$$mn\frac{d\mathbf{v}}{dt}=qn\mathbf{E}-\nabla p-mn\nu_m\mathbf{v}, \tag{1}$$

where m is the mass of the particle, n is the density, $\mathbf{v}$ is the velocity, q is the charge, E is the electric field, p is the pressure, and ν_m is the collision frequency. The three terms in the right-hand side of Eq. (1) are the electric field, pressure gradient, and frictional forces. Since the characteristic time of the fast relaxation of the electron density is much longer than the time for momentum loss in collision, Eq. (1) describing the motion of the electrons can be simplified to Eq. (2),

$$en\mathbf{E}+\nabla p+mn\nu_m\mathbf{v}=\mathbf{0}. \tag{2}$$

In the laser impact region, the pressure gradient is so large that the friction term can be neglected, i.e., E and p can be described by

$$en\mathbf{E}\approx-\nabla p. \tag{3}$$

In other words, the pressure gradient at the edges of the laser impact region creates the self-consistent electric field, in order to lower the electron flux. After integrating Eq. (3), the well-known Boltzmann relation can be obtained. Since the pressure gradient ∇p has an opposite sign at the edges of the laser impact region, also the electric field will change sign [see Fig. 2(b)].

The created self-consistent electric field in the laser impact region reflects a potential well for electrons, which ''traps'' detached electrons in the laser impact region, and thereby, preserves quasineutrality in the plasma [15]. The depth of the potential well W is predicted as $W\approx\varepsilon_0$ [15], where ε_0 is the difference between the laser photon energy and the electron affinity. In our case, $\varepsilon_0=0.2$ eV, which corresponds to a drop of the electric field of some hundreds volts per meter. This field can be seen at the laser impact region after one rf cycle in Fig. 2(b). Since the electrons leave the laser impact region gradually, the depth of the potential well, will become shallower [compare the local field after five rf cycles with that after one rf cycle in Fig. 2(b)]. The potential well is expected to disappear after R/v_- [15], where R is the laser radius and v_- is the averaged thermal velocity of negative ions.

At the outside of the laser impact region, the electron density gradient, i.e., the pressure gradient can be neglected, compared with the electric field and the friction forces, i.e., the macroscopic motion Eq. (2) is simplified to Ohm's law,

$$-en\mathbf{v}=\mathbf{j}=\frac{e^2n\mathbf{E}}{m\nu_m}=\sigma\mathbf{E}, \tag{4}$$

where $\mathbf{j}$ is the current density and σ is the conductivity. Since the mobility of electrons is much higher than the ions, the current is carried mainly by electrons. In strongly electronegative discharges, the electron density is low (much lower than the negative ion and positive ion densities), hence the electric field is rather strong [21,22] in order to achieve the same current density. This strong field is clearly shown by the electric field value (about 1300 V/m at zero rf cycle) before photodetachment and by the almost unchanged part close to the presheaths (dashed line) in Fig. 2(b). The strong drop of the electric field out of the laser impact region [see the curves after one rf cycle and five rf cycles in Fig. 2(b)] results from the increase of the electron density over there. The electrons come from the laser impact region by diffusion, because from Eq. (4) it can be obtained that the electric field has to be low with the increase of the electron density in order to keep the continuity of current in the discharge.

In this fast change period, the net charge density profile varies strongly and violates the local quasineutrality (see Fig. 4). Note that the integrated net charge density over the plasma bulk region still keeps neutrality. The net charge density around the laser impact region after one rf cycle (dashed line) deviates strongly from the quasineutral line marked by circles. This oscillation may be due to the fact that the initial Maxwellian electron distribution is perturbed by the monoenergetic distribution of detached electrons, and that a change in the electron density may provoke electrostatic oscillations, especially if the time scale $\tau_{\Delta ne}$ for the increase in the detached electron density is shorter than the time scale of

plasma oscillation ${\omega_{pe}}^{-1}$ [2,7]. In our case, $\tau_{\Delta ne}=0$. Even if the laser pulse duration is considered, normally it is about 10 ns, the condition of $\tau_{\Delta ne} \leqslant {\omega_{pe}}^{-1}$ is easily satisfied in our case (${\omega_{pe}}^{-1} \approx 74$ ns). The oscillation starts from the edges, then damps quickly and propagates toward the presheaths. As shown in the net charge density profile after five rf cycles, the deviations of the net charge density at the laser impact region decrease, but they appear at presheaths (see the solid line in Fig. 4). This electrostatic oscillation is caught up by using our self-consistent model. Previous models [4–7] used charge neutrality as an assumption, therefore, this phenomenon could not be seen. Furthermore, in strongly electronegative discharges this phenomenon is much stronger compared to that in weakly electronegative discharges because of the large density gradient in the former case. Note that in the current situation the laser intensity has a simple rectangular shape, therefore, from a theoretical point of view the density gradient is infinite. However, in the numerical simulation, i.e., the PIC/MC model, the density of electrons is treated as weighing the number of electrons in a certain cell, on the adjacent grid points of this cell [16]. In other words, the density value at each grid point is averaged over the number of electrons in the adjacent two cells. As a result, the density gradient of the electrons is not infinite in our simulation. As mentioned in the assumption, the laser intensity profile in our case is a rectangular or a tail-cut Gaussian distribution, hence this oscillation phenomenon is strong. However, if the laser intensity profile keeps the Gaussian distribution and if the laser intensity is not large enough to depopulate the negative ions entirely, the density gradient will not be so strong, hence, the phenomenon of the oscillation observed here will become weak.

c. Period of large changes. From ''*b*'' to ''*c*'' in Fig. 1 (about 40 rf cycles), the local electron density drops closely to its original value, by diffusing away from the laser impact region. The dip of the SiH_3^- density is filled up to 80% of its original value, by diffusing toward the laser impact region from the surrounding area.

The local positive ion density also strongly varies during this period. When the difference of the diffusion fluxes of electrons and negative ions affects the center of the laser impact region, the local positive ion densities at the center have to drop, in order to keep the charge neutrality. Consequently, sharp dips occur at the center in the SiH_3^+ and H_2^+ densities profiles (e.g., see Fig. 3). The dip in the H_2^+ density profile after 20 rf cycles is illustrated by a solid line in Fig. 3. The H_2^+ ion density shows a pronounced drop (to 40% of its original value in the middle of the laser impact position). It is also clear from Fig. 1 that the H_2^+ density decreases more rapidly than the SiH_3^+ density due to its lighter mass. Note that the amount of the drop of the positive ions is more or less equal to the loss of the negative ions due to photodetachment. These ''extra'' positive ions follow the diffusion of the extra electrons and get lost to the walls [8] to balance the decrease of negative ions by photodetachment and the fast loss of the extra electrons to the walls.

With more and more extra electrons smearing out, near point ''$a1$'' moment (in the evolution of the local H_2^+ density in Fig. 1) the gradient of the e^- density at the laser impact region becomes small, and hence, the recovery speed of the e^- density slows down. In the meanwhile, the electric field (the potential well for electrons) created to balance the electron density gradient also becomes weak and eventually it changes its sign. This change of sign in the field results from the fact that the diffusion flux of the negative ions becomes stronger than that of the electrons. The change of sign can be seen from the fact that the electric fields around the laser impact region after 27 cycles and after five rf cycles in Fig. 2(b), are symmetric relatively to the zero electric field line. Influenced by this field and by the large density gradient, the positive ions around the laser impact region are pushed back to the center and start to fill up the dip in their density profiles. This is demonstrated by the line marked by circles in Fig. 3 (after 35 rf cycles vs 20 rf cycles). In other words, the positive ions change their direction of motion from following the electrons to following the negative ions. The point of change from the decreasing phase to the increasing phase in the recovery of H_2^+ density occurs after about 20 rf cycles, which corresponds to the minimum in the evolution curve of the H_2^+ density in Fig. 1 (marked by ''$a1$''). The minimum at the point ''$b1$'' for the local SiH_3^+ density appears somewhat later than that for the H_2^+ density because of a higher mass and hence slower motion, and the minimum for the total positive ion density is marked by ''$c1$'' after about 27 rf cycles.

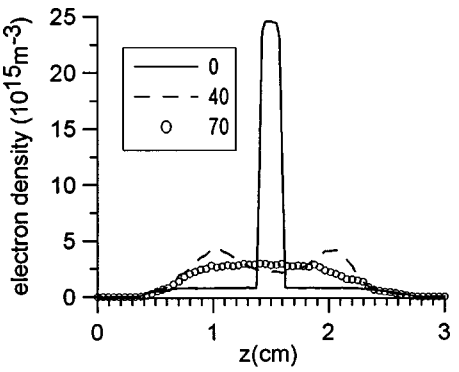

FIG. 5. Electron density profile after 0, 40, and 70 rf cycles.

The electric field that has now opposite sign (i.e., a potential hill for electrons), will reduce the flux of negative ions toward the center and increase the flux of electrons toward the presheaths. As a result, the local electron density decreases further from the moment corresponding to point ''$c1$'' to the moment corresponding to point ''*c*.'' A dip corresponding to point ''*c*'' in Fig. 1 appears in the electron density profile, see the curve after 40 rf cycles in Fig. 5, where the electron density profile at different moments in time is shown.

The dip in the recovery process of the local positive ion density, similar to that shown in Fig. 1, has indirectly been experimentally observed in [7,9] by the sum of the local electron density and the local negative ion density taking into account the requirement for the charge neutrality. This dip has been observed appearing at the same moment in time as the overshoot in the electron current pulse in experiments [9,10,12,13]. The overshoot is explained by the departure of positive ions from the laser irradiated volume. As a result the

electron density decreases below its initial steady-state value in order to maintain the plasma neutrality, before returning to the steady-state value [9]. The overshoot is expected to appear when the positive ion density drops strongly and $\alpha = \sqrt{\gamma T_+ / T_e}$ is small, where γ is the adiabatic index, and T_+ and T_e are the temperatures of the positive ions and electrons, respectively. In our case, the drop in the positive ion density profile is rather large, about 60% of its original value (see Fig. 3) and $\alpha = 0.35$ is in the overshoot expected range. However, we could not see the overshoot in the recovery process of the local electron density. Only a dip in the local electron density is found at point "*c*" in Fig. 1, and it is still above the original density. From our results, this dip does not result from the departure of positive ions from the laser impact region, but it results from the change in sign of the created electric field as mentioned above. During the formation process of the dip in the local electron density, the positive ions move back to the laser impact region. From our results, an overshoot may occur when the positive ions move back slowly and the electrons are strongly pushed away by the created self-consistent field to compensate for the relatively larger flux of negative ions at this period in time.

d. Period of slow recovery. After point "*c*," all the charged particle densities recover slowly. The inward diffusion of the negative ions and the positive ions becomes negligible because of the lower density gradients. Since the negative and positive ion fluxes almost balance each other, the electron density will not decrease further. On the contrary, due to inward diffusion, the electrons from the surrounding area will fill up the dip at the laser impact position, as demonstrated in Fig. 5 (see the density profile after 70 rf cycles vs 40 rf cycles). Consequently the local electron density experiences a local maximum at point "*d*" (after 70 rf cycles) in Fig. 1.

With the slow recovery of ions, the somewhat increased local electron density finally decays again and recovers completely to its original value at point "*e*" (after 200 rf cycles in Fig. 1). The relaxation process from "*d*" to "*e*" is closely related to the recovery of the local electric field, see Fig. 2(a). This confirms the prediction that a long lasting potential structure, whether positive or negative, should be associated with perturbations in electron density [3]. After point "*c*," the recovery of ions mainly depends on the small net increment between the production and the loss, hence it will take a very long time, and it is not yet finished at point "*e*," where the electron density has recovered [8].

B. Relaxation of local energy

Only the local energy relaxation of the electrons and negative ions is studied here. The influence of the photodetachment on the energy of the local positive ions is very small, and is not shown here.

1. Energy relaxation of the electrons

Figure 6 shows the local EEDF (i.e., at the laser impact position) at several moments in time. The energy step is 0.05 eV. The peak at 0.2 eV in Fig. 6 corresponds to the extra electrons created after photodetachment (see above in the assumption). The EEDF appears to change dramatically by photodetachment as is presented by the dashed line in Fig. 6 (i.e., after 30 rf cycles). The decrease of the high-energy tail of the EEDF is due to the weakened electric field (see Fig. 2). The broadening of the peak (at 0.2 eV) towards high energy, i.e., the broadened part between 0.2 eV and 1 eV, can be understood because the high-energy electrons (higher than 1 eV) lose energy due to collisions, hence leading to an energy shift to low energy. The broadening of the peak (at 0.2 eV) towards low energy, i.e., the broadened part at less than 0.2 eV, is due to vibrational excitation collisions with threshold energy of 0.11 eV. The shape shown after 30 rf cycles in Fig. 6 is kept more or less the same until the local electric field starts to recover after 100 rf cycles. Later on, the low-energy part of the EEDF drops due to the outward diffusion of 0.2 eV detached electrons, while the high-energy tail rises due to heating by the gradually recovered electric field. These two processes go synchronously, and after 220 rf cycles (the line marked by circles), the local EEDF has recovered to nearly the original shape.

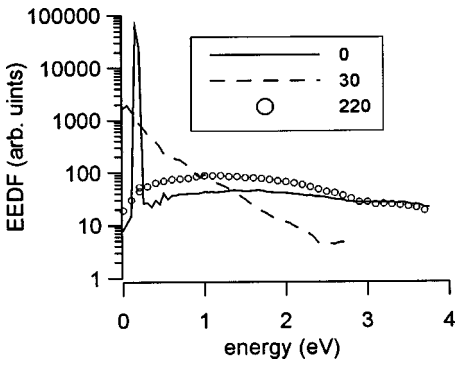

FIG. 6. EEDF at the laser impact region after 0, 30, and 220 rf cycles.

Figure 7 shows the evolution of the average energy of the electrons, ε_e, at the laser impact position. It can be seen that the evolution of the electron energy has a quite similar behavior to that for the local electric field [Fig. 2(a)]. It can be understood as follows.

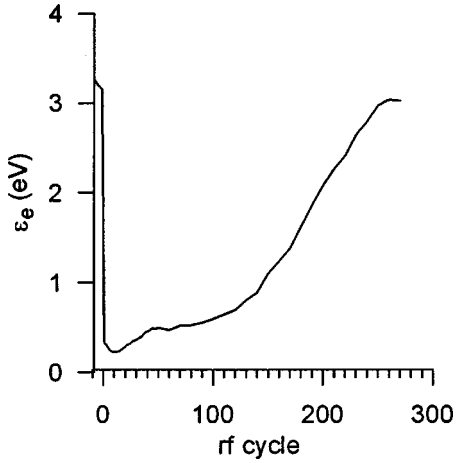

FIG. 7. Evolution of the average electron energy at the laser impact position as a function of number of rf cycles.

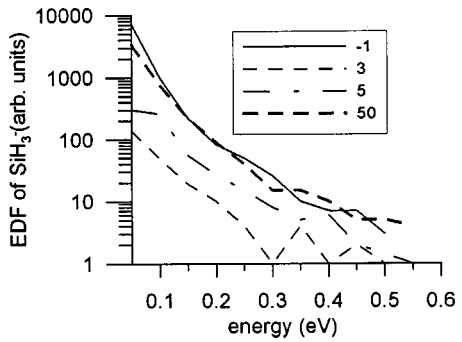

FIG. 8. EDF of SiH_3^- ions at the laser impact region after -1, 3, 5, and 50 rf cycles. (''-1 rf cycle'' means one rf cycle before photodetachment takes place).

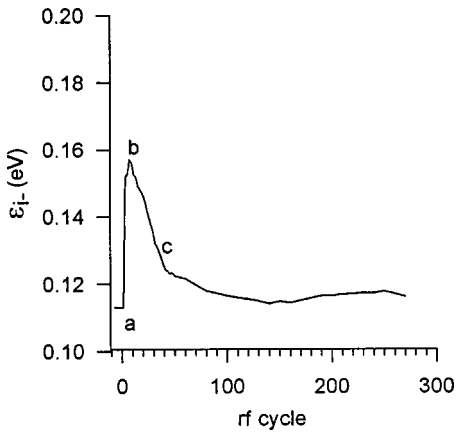

FIG. 9. Evolution of the average energy of SiH_3^- as a function of number of rf cycles at the laser impact position. The letters *a*, *b*, *c* indicate different moments in time.

(1) The ratio of the detached electrons to the original electrons (i.e., before photodetachment) is about 16:1, therefore, the contribution of the original electrons to the average electron energy can be neglected, even at the very beginning. Hence, just after photodetachment, the average electron energy drops to about 0.2 eV, which is assumed to be the energy of the detached electrons.

(2) In a very short time (about 40 rf cycles) the electron density decreases drastically to a steady value, close to its original one (see Fig. 1). It would be expected that the small number of electrons left benefit, by electron heating, from the quick drop in the electron density. However, since the electric field is close to zero [see points ''*b*'' to ''*c*'' in Fig. 2(a)], it cannot quickly heat up the low-energy electrons in order to compensate for the loss of the high-energy electrons by outward diffusion and by collisions. Therefore, the increase of the average electron energy does not behave like what is expected (i.e., benefiting by electron heating from the quick drop of the electron density). The average electron energy is still rather low in this period.

(3) Later on, when the local electron density reaches its steady-state value, the change of the local electron energy mainly depends on the evolution of the local electric field.

The recovery of the local electron energy reflects the process that the detached electrons with very low energy (0.2 eV) follow the evolution of the local electric field gradually to be heated up to their original distribution function. Thus, the recovery of the local electron energy resembles that of the electric field.

It is clear from Figs. 6 and 7 that it will take a rather long time for the energy distribution of electrons after photodetachment to return back to its original value, because the energy obtained by the large amount of extra electrons mainly depends on the heating by the local electric field and the electric field is strongly weakened. This point is quite different from the recovery of the distribution of electrons in weakly electronegative discharges, e.g., [2,5,7], where the amount of the created electrons is too small to influence the electric field.

2. Energy relaxation of the negative ions

The energy recovery of the negative ions is quite different from that of the electrons. Figure 8 shows the EDF of SiH_3^- at the laser impact position at several moments in time. Note that the EDF of SiH_3^- at the moment just after photodetachment is not shown here, because there are no negative ions in the laser impact region at this moment. Instead, the EDF of SiH_3^- just before photodetachment takes place (i.e., indicated as ''-1'' rf cycle), is illustrated by the solid line. From Fig. 8, it can be seen that the EDF of SiH_3^- recovers rather quickly due to the strong diffusion of SiH_3^- from the surrounding area of the dip. After 50 rf cycles, the tail of the EDF is very close to the original value, but the low-energy part still needs to recover. At this moment, the diffusion becomes small and the recovery will rely on the increment of the production of SiH_3^- ions through the electron attachment collisions.

The relaxation of the average negative ion energy (ε_{i-}) at the laser impact position is shown in Fig. 9. The relaxation process of ε_{i-} can be subdivided into different phases. We use different letters to mark the transition between two adjacent phases in Fig. 9. The tendency of the evolution of ε_{i-} is quite different from that of the electrons and of the local electric field, because the local average energy of the negative ions is influenced not only by the local electric field, such as in the electron case, but also by the penetration of the negative ions, by inward diffusion. Combining these two facts, the recovery behavior of ε_{i-} in Fig. 9 can be understood as follows:

(1) At point ''*a*,'' ε_{i-} is in fact not defined because there are almost no negative ions at the laser impact position at this moment. We assume that it has the same value as before the photodetachment.

(2) From ''*a*'' to ''*b*'' (excluding ''*a*''), the pronounced increase of ε_{i-} is due to the penetration of few SiH_3^- ions with high energy, and due to the acceleration by the created self-consistent field.

(3) From ''*b*'' to ''*c*,'' ε_{i-} clearly decreases. This results from the arrival of the large amount of slow negative ions and from the gradually weakened and even the sign-changing self-consistent electric field [see the local field after 27 cycles in Fig. 2(b)]. The characteristic time (τ_-) of negative ions traveling a distance equal to the radius (R) of the

laser beam with thermal velocity can be estimated by $\tau_- = R/\sqrt{2KT_-/m_-}$, where T_- is the negative ion temperature and m_- is the mass of the negative ions. In our case, τ_- is about 1.2 μs. From the moment corresponding to point "*c*" in Fig. 9, it can be obtained that after about 35 rf cycles, i.e., after 2.6 μs, the local averaged energy of the negative ions returns closely to its original value. This difference between the estimated (1.2 μs) and the calculated time (2.6 μs) is due to the created self-consistent field in the practical recovery process and due to the change of the sign of this field, which slows down the penetration of the negative ions.

It is clear from Fig. 9 that the influence of photodetachment on the negative ion energy is only important during the phase from "*a*" to "*c*." In the remaining time, the influence can be ignored. This result confirms the prediction and analysis of previous theoretical work [7] that the early potential perturbation can distort the measurement of negative ion temperature and results in a relatively higher value than the real temperature. The authors [7], therefore, suggested to use the phase after the potential perturbation to determine the temperature of negative ions. In our case this phase starts after point "*c*" in Fig. 9.

IV. CONCLUSIONS

The relaxation phenomena at the laser impact position after photodetachment are studied with a 1D self-consistent PIC/MC model. A SiH_4/H_2 discharge is chosen as an example to demonstrate the relaxation phenomena of the charged particle (e^-, SiH_3^+, H_2^+, and SiH_3^-) densities and energies, of the electric field and of the net charge density, typical for strongly electronegative discharges.

From the results, we can confirm some theoretical predictions in the relaxation process: (1) the potential well (the self-consistent electric field) created by the difference of the fluxes between electrons and negative ions at the laser impact region [2,7,15]; (2) the electrostatic oscillation [2,7] in the net charge density profile due to the sudden change of electron density; (3) the long lasting potential structure associated with perturbations in the electron density [7]; (4) the distortion of the early potential perturbation on the measurement of negative ion temperature [7]; and (5) the depression in the positive ion density at the edges of the laser impact region [5].

We also point out the difference in the local relaxation between weakly and strongly electronegative discharges. In the latter kind of discharges, the recovery of electron energy and EEDF takes a long time. The electric field has been weakened strongly after photodetachment, and it relaxes with the recovery of the local electron density. The electrostatic oscillation is very strong and continues over several rf cycles in our case, as appears from the strong deviation from quasineutrality in the net charge density profile. The local positive ions respond to the strongly created self-consistent field within the time scale of one rf cycle.

A large dip in the center of the positive ion density profile, observed in the experiment, is found and explained. However, no overshoot of the local electron density is found. A possible reason is that in our simulations the discharge conditions and the gas components are different from those in experiments [9,11,12], where such an overshoot has been observed. To explain experimental observations an extensive scan of discharge parameters is required, which needs a large computational effort and is beyond the scope of this paper.

ACKNOWLEDGMENTS

M.Y. is financed by a New Research Initiative of the University of Antwerp and by the Bilateral scientific and technological cooperation (joint Project No. BIL 99/46) of the Ministry of the Flemish Community, the Ministry of Science and Technology of China, and the National Science Foundation of China. M.Y. gratefully acknowledges discussions with D. Hayashi and B. Kuvshinov. A.B. is indebted to the Flemish Fund for Scientific Research (FWO) for financial support. The PIC/MC code was developed with financial support from The Netherlands Organization for Scientific Research (NWO). The authors also acknowledge financial support from the Belgian Federal Services for Scientific, Technical, and Cultural Affairs (DWTC/SSTC) of the Prime Minister's Office through IUAP-IV (Conv. P4/10).

[1] M. Bacal, Plasma Sources Sci. Technol. **2**, 190 (1993).
[2] M. Bacal, Rev. Sci. Instrum. **71**, 3981 (2000).
[3] R. A. Stern, P. Devynck, M. Bacal, P. Berlemont, and F. Hillion, Phys. Rev. A **41**, 3307 (1990).
[4] L. Friedland, C. I. Ciubotariu, and M. Bacal, Phys. Rev. E **49**, 4353 (1993).
[5] A. A. Ivanov, L. I. Elizarov, M. Bacal, and A. B. Sionov, Phys. Rev. E **52**, 6679 (1995).
[6] A. A. Ivanov, A. B. Sionov, C. I. Ciubotariu, and M. Bacal, Phys. Rep. **24**, 965 (1998).
[7] D. A. Skinner and C. Couteille, Phys. Plasmas **1**, 2785 (1994).
[8] M. Yan, A. Bogaerts, R. Gijbels, and W. Goedheer, Phys. Rev. E **63**, 026405 (2001).
[9] P. Devynck, J. Auvray, M. Bacal, P. Berlemont, J. Bruneteau, R. Leroy, and R. A. Stern, Rev. Sci. Instrum. **60**, 2873 (1989).
[10] M. Bacal, P. I. Berlemont, A. M. Bruneteau, R. Leroy, and R. A. Stern, J. Appl. Phys. **70**, 1212 (1991).
[11] D. Hayashi and K. Kadota, J. Appl. Phys. **83**, 697 (1998).
[12] M. Nishiura, M. Sasao, and M. Bacal, J. Appl. Phys. **83**, 2944 (1998).
[13] M. Nishiura, M. Sasao, M. Wada, and M. Bacal, Phys. Rev. E **63**, 036408 (2001).
[14] M. Yan and W. J. Goedheer, IEEE Trans. Plasma Sci. **27**, 1399 (1999).
[15] F. EI Balghiti-Sube, F. G. Baksht, and M. Bacal, Rev. Sci. Instrum. **67**, 2221 (1996).
[16] C. K. Birdsall, IEEE Trans. Plasma Sci. **19**, 65 (1991).
[17] V. Vahedi and M. Surendra, Comput. Phys. Commun. **87**, 179 (1995).

[18] E. Hamers, Ph.D. thesis, Utrecht University, The Netherlands, 1998.
[19] G. J. Nienhuis and W. J. Goedheer, J. Appl. Phys. **82**, 2060 (1997).
[20] J. Perrin, J. Perrin, O. Leroy, and M. C. Bordage, Contrib. Plasma Phys. **36**, 3 (1996).
[21] M. Yan, A. Bogaerts, R. Gijbels and W. J. Goedheer, J. Appl. Phys. **87**, 3628 (2000).
[22] T. J. Sommerer, W. N. G. Hitchon, R. E. P. Harvey, and J. E. Lawler, Phys. Rev. A **43**, 4452 (1991).